25th ABCM International Congress of Mechanical Engineering
October 20-25, 2019, Uberlândia, MG, Brazil

COBEM2019-0957
THEORETICAL AND NUMERICAL NONLINEAR DYNAMIC STUDY OF THE VON MISES STRUCTURE

Lucas Sardinha de Arruda[1]
Reyolando Manoel Lopes Rebello da Fonseca Brasil[2]
[1]Universidade de São Paulo, Av. Prof. Almeida Prado, trav.2 nº. 83 Cidade Universitária, 05508-900, São Paulo, São Paulo, Brazil.
[2]Universidade Federal do ABC, São Bernardo, Brazil, Alameda da Universidade, s/n, Bairro Anchieta, 09606-045, São Bernardo do Campo, São Paulo, Brazil.
[1]arrudalucas@usp.br
[2]reyolando.brasil@ufabc.edu.br

Abstract. *A nonlinear numerical study of the von Mises structure was carried out to describe its dynamic behavior under a set of distinct load histories, since it is well known that this problem may lead, for certain parameters and initial conditions, to chaotic solutions, among other rich dynamic behaviors. In addition, a pseudo-static analysis using different cross-sections, material and load conditions is developed to obtain the characteristic dynamic snap-through phenomenon present in literature. The numerical algorithm is written in MATLAB© language and based on a 'composite scheme', where the first sub-step solution is obtained via the trapezoidal rule, and for the second sub-step solution, a 3-point Euler backward formula is employed. The dynamic equilibrium at each load step is achieved via a path following methodology, seeking to solve the nonlinear systems of equations derived from the time integration procedure. This combination of numerical procedures seeks to describe the exact structural dynamic behavior at every load step, as well as ensuring the convergence of the method for nonlinear problems.*

Keywords: *Nonlinear dynamic analysis, Nonlinear truss element, von Mises truss.*

1. INTRODUCTION

The von Mises structure consists of two identical truss elements, loaded with a vertical force r_o at the central node and simply supported at the other ends, as shown in Fig. 1, where the vertical displacement at the central node at any instant is given by $w = a + u(t)$, where a is the bar's height at its initial configuration and $u(t)$ the displacement variable. This simple two-element truss model is traditionally used to illustrate the geometric non-linear behavior of structures (Crisfield (1991), Krenk (2009) and Reddy (2004)), as well as a benchmark for nonlinear static procedures due to its well-known load-displacement curve. Furthermore, in the dynamic context, it is well known that this problem may lead, for certain parameters and initial conditions, to chaotic solutions, among other rich dynamic behaviors.

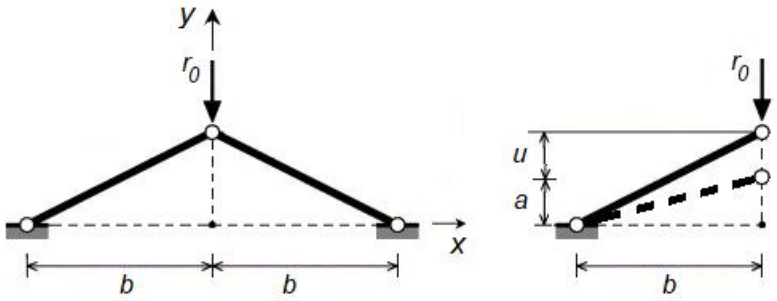

Figure 1. A two-element truss von Mises model, Ligarò (2006).

The two bars are initially assumed to be linear elastic, with cross section area A, elastic modulus E and initial length l_0. Additionally, the structure is assumed to be shallow, that is, $a \ll b$ and consequently, θ is small. The vertical equilibrium of the central node in the deformed state requires that the external force r_o be equals to the restoring internal elastic force, $f_{int}(u)$, generated by deformation of the structure. Thus,

$$r_o = f_{int}(u) = 2N \sin\theta = 2N(u+a)/l \sim 2N(u+a)/l_o \tag{1}$$

	m	Strain	Stress
Almansi	-2	$\varepsilon_A = \frac{1}{2}(1-\lambda^{-2})$	$\sigma_A = \sigma_N \lambda^3$
Hiperbolic	-1	$\varepsilon_H = 1-\lambda^{-1}$	$\sigma_H = \sigma_N \lambda^2$
Logarithmic	0	$\varepsilon_L = \ln(\lambda)$	$\sigma_L = \sigma_N \lambda$
Linear	1	$\varepsilon_N = (\lambda - 1)$	$\sigma_N = N/A$
Green	2	$\varepsilon_G = \frac{1}{2}(\lambda^2 - 1)$	$\sigma_G = \sigma_N \lambda^{-2}$

Figure 2. Deformation family and stress conjugated measures, Driemier et.al. (2004).

The deformation of the bars is described by their elongation λ and may be written using a series of deformations and stress conjugated measures, as shown in Fig. 2. Adopting as measure of deformation the engineering strain, ε_N, defined as the elongation relative to the original length, we have:

$$\varepsilon_N = \lambda - 1 = (l - l_0)/l_0 \sim (au + 0.5u^2)/l_0^2 \tag{2}$$

The axial force in each bar is expressed in terms of the strain as,

$$N = \sigma_N A = EA(au + 0.5u^2)/l_0^2 \tag{3}$$

Substituting the axial force, Eq. (3), in the vertical equilibrium equation, Eq. (1), we can write the relationship between the external force r_o and the displacement u, as

$$r_o = 2(EA(au + 0.5u^2)/l_0^2)((u+a)/l_o) = (2EA/l_0^3)(a^2u + 1.5au^2 + 0.5u^3) \tag{4}$$

Equation (4) can be easily expanded to consider the dynamic effects. For this, we consider only symmetric motions of the system, which implies that the central node can only move vertically, that the structure's mass is entirely lumped at the junction between the two bars, and a linear viscous dissipation model. Under these considerations, the equation of motion may be written, for a periodic excitation, as,

$$m\ddot{u} + c\dot{u} + (2EA/l_0^3)(a^2u + 1.5au^2 + 0.5u^3) = r_o \cos(\omega t) \tag{5}$$

To better study the nonlinear effects in the dynamic context, Eq. (4) and Eq. (5) can be rewritten in non-dimensional form as

$$\eta = x + 1.5x^2 + 0.5x^3 \tag{6}$$

$$\ddot{x} + \xi\dot{x} + \alpha(x + 1.5x^2 + 0.5x^3) = \gamma \cos(\Omega\tau) \tag{7}$$

where $\eta = -r_0(l_0/a)^3/EA$ and $x = u/a$ are the non-dimensional load and displacement parameters used in Eq. (6), respectively. And $\tau = tw_0$, $\Omega = w/w_0$, $w_0^2 = 2EA/ml_0$, $\gamma = r_0/mw_0^2$, $\xi = c/mw_0$ and $\alpha = (a/l_0)^2$ are the additional non-dimensional parameters required by the dynamic equation of motion, Eq. (7).

2. METHODS

2.1 Time integration procedure.

The implemented "composite" time integration scheme was proposed by Bathe (2007) as an alternative to the classic Newmark method for large displacements and long dynamic responses structural analysis. The main idea behind this scheme is calculate the unknown variables by considering the time step Δt as two equally sized sub-steps. In the first sub-step, the Newmark constant average acceleration method is used to compute the variables value at $t + \Delta t/2$. Then, this solutions in employed in the 3-point Euler backward formula to obtain the new equilibrium state at $t + \Delta t$. In other words, the method uses the solution obtained from the Newmark method as an additional information for the Euler backward formula, correcting and improving its results. For this reason, this simple and efficient procedure is a second-order

accurate scheme with small amplitude decay and period elongation and can be directly employed when the mechanical energy is not conserved.

Assuming that for a n-set of nonlinear equilibrium equation with fixed mass matrix $\boldsymbol{m}$ and damping matrix $\boldsymbol{c}$, the dynamic equilibrium at the end of a time step $t + \Delta t$ may be expressed as Eq. (8).

$$\boldsymbol{m}\ddot{\boldsymbol{u}}_{tf} + \boldsymbol{c}\dot{\boldsymbol{u}}_{tf} + \boldsymbol{f}_{int} = \boldsymbol{f}_{ext} \tag{8}$$

where $\boldsymbol{f}_{ext}$ is the equivalent external forces. In the first sub-step, the nodal variables at time $t + \Delta t/2$ are computed via an iterative scheme using the following relation.

$$\left(\frac{16}{\Delta t^2}\boldsymbol{m} + \frac{4}{\Delta t}\boldsymbol{c} + \boldsymbol{k}_T^{i-1}\right)_{t+\Delta t/2} \Delta\boldsymbol{u}^{\boldsymbol{i}} = \left(\boldsymbol{f}_{ext} - \boldsymbol{f}_{int}^{i-1}\right)_{t+\Delta t/2} - \boldsymbol{m}\left(\frac{16}{\Delta t^2}\left(u_{t+\Delta t/2}^{i-1} - u_t\right) - \frac{8}{\Delta t}\dot{u}_t - \ddot{u}_t\right) - \boldsymbol{c}\left(\frac{4}{\Delta t}\left(u_{t+\Delta t/2}^{i-1} - u_t\right) - \dot{u}_t\right) \tag{9}$$

where $u_{t+\Delta t/2}^{i} = u_{t+\Delta t/2}^{i-1} + \Delta u^{i}$. Thereafter, the second sub-step requires the solution of the previous equilibrium point (t) and the nodal variables at time $t + \Delta t/2$ to obtain the increment displacement at time step $t + \Delta t$ via an iterative scheme using the 3-point backward Euler method, as follows.

$$\left(\frac{9}{\Delta t^2}\boldsymbol{m} + \frac{3}{\Delta t}\boldsymbol{c} + \boldsymbol{k}_T^{i-1}\right)_{t+\Delta t} \Delta\boldsymbol{u}^{\boldsymbol{i}} = \left(\boldsymbol{f}_{ext} - \boldsymbol{f}_{int}^{i-1}\right)_{t+\Delta t} - \boldsymbol{m}\left(\frac{9}{\Delta t^2}u_{t+\Delta t}^{i-1} - \frac{12}{\Delta t^2}u_{t+\Delta t/2} + \frac{8}{\Delta t^2}u_t - \frac{4}{\Delta t}\dot{u}_{t+\Delta t/2} + \frac{1}{\Delta t}\dot{u}_t\right) - \boldsymbol{c}\left(\frac{3}{\Delta t}u_{t+\Delta t}^{i-1} - \frac{4}{\Delta t}u_{t+\Delta t/2} + \frac{1}{\Delta t}u_t\right) \tag{10}$$

2.2 Incremental-iterative numerical procedure.

Typically, the set of equilibrium equations at each time step is solved via a predictor-corrector scheme based on the Newton-Raphson method. However, there are some occasions when this kind of approach is inefficient, especially when dealing with large nonlinearities, such as regions near limit points or snap-through/snap back conditions. For this reason, we chose to implement an algorithm based on a path-following strategy, such as the Orthogonal residual algorithm or the Arc-length algorithm. The latter is used in this work.

The main idea behind the Arc-length method is to propose additional constraints that aims to find the intersection between the governing equations and an n-dimensional sphere with a fixed radius Δl, thus turning the whole system into a solvable one. In the spherical version of the method, this constraint is given by,

$$\Delta\boldsymbol{u}^T\Delta\boldsymbol{u} + \Delta\lambda^2\varphi^2\boldsymbol{f}_{ext}{}^{\boldsymbol{T}}\boldsymbol{f}_{ext} - \Delta l = 0 \tag{11}$$

where $\Delta\boldsymbol{u}$ is the incremental displacement, $\Delta\lambda$ the incremental load factor and φ the scaling parameter. The main idea behind this approach is illustrated in Fig. 3.

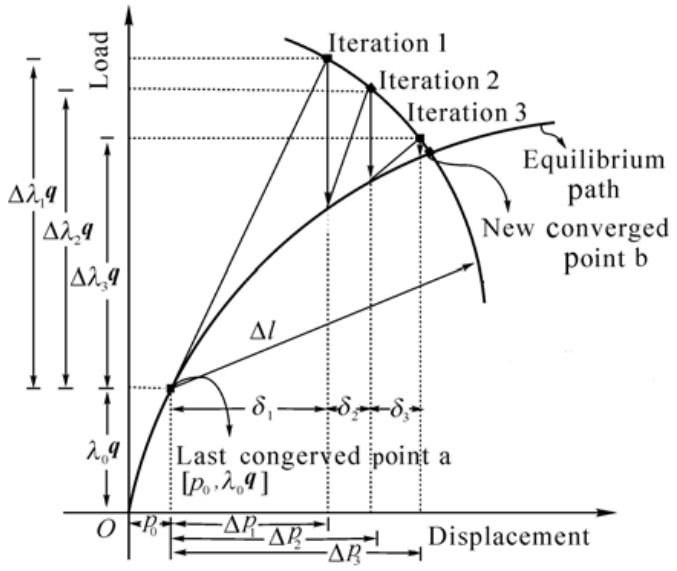

Figure 3. Arc-length methodology based on Newton-Rhapson method, Crisfield (1991).

In Figure 3, from a previous equilibrium point (point A), we determine an initial displacement increment δu_t^i based on a tangent estimative (same as the classic Newton-Raphson procedure), leading to the Tangential solution from point A. This initial guess is then corrected by an iterative process based on the constraint equation Eq. (11) until the final solution is achieved.

2.3 Nonlinear truss element.

Assuming a generic truss bar element in its global reference frame, as shown in Fig. 4, we designate V^s, A^s and l^s as its volume, cross section area and length in state s - either the reference state or the current one.

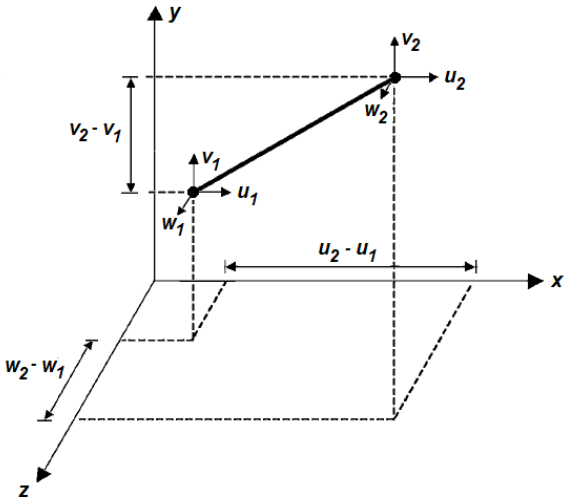

Figure 4. Truss element bar in the global reference frame, Driemier et.al. (2004).

In this configuration, the element nodal array is presented as,

$$\boldsymbol{x}_e = \{\{x, y, z\}_1, \{x, y, z\}_2\}^T \tag{12}$$

where $\{x, y, z, \}_{i=1,2}$ refers to each set of nodal coordinates. The element length l^s and its stretch λ^* can be then determined using the following relations:

$$l^s = \boldsymbol{x}_e^T \boldsymbol{\phi}^T \boldsymbol{\phi} \boldsymbol{x}_e \tag{13}$$

$$\lambda^* = (l^{crt}/l^{ref}) = (\sqrt{\boldsymbol{x}_e^T \boldsymbol{\phi}^T \boldsymbol{\phi} \boldsymbol{x}_e})/l^{ref} \tag{14}$$

where $\boldsymbol{\phi}$ is a matrix relating the two element nodes and given by $\boldsymbol{\phi} = [-\boldsymbol{I}_3 \quad +\boldsymbol{I}_3]$, with $\boldsymbol{I}_3$ representing the 3x3 identity matrix; the superscripts ^{crt} and ^{ref} are related to the current state and the reference one, respectively. Adopting a linear constitutive relation and a family of strain relations, it is possible to derive the element internal force and stiffness matrix, given by:

$$\boldsymbol{f}_{int,e} = V^{ref} \sigma^m \lambda^{*2m} (l^{crt})^{-2} \boldsymbol{\phi}^T \boldsymbol{\phi} \boldsymbol{x}_e \tag{15}$$

$$\boldsymbol{K}_{T,e} = V^{ref} \lambda^{*4m} (l^{crt})^{-4} E \boldsymbol{\phi}^T (\boldsymbol{\phi} \boldsymbol{x}_e)(\boldsymbol{\phi} \boldsymbol{x}_e)^T \boldsymbol{\phi} + V^{ref} \lambda^{*2m} [(2m-2) l^{crt^{-4}} \sigma^m \boldsymbol{\phi}^T (\boldsymbol{\phi} \boldsymbol{x}_e)(\boldsymbol{\phi} \boldsymbol{x}_e)^T \boldsymbol{\phi} + l^{crt^{-2}} \sigma^m \boldsymbol{\phi}^T \boldsymbol{\phi}] \tag{16}$$

where E is the elastic modulus of the structure (the procedure can be easily adapted to be a piecewise elastic tangent modulus of a material nonlinear model) and m a parameter related to the strain-stretch relation (for example, $m = 1/2$ denotes the linear strain relation, while $m = 1$ lead to the Green's strain relation).

2.4 Nonlinear material model.

The proposed nonlinear material model is based on the One-Dimensional J2 (von Mises) Plasticity theory presented in Conte (2003). In this approach, the one-dimensional total strain ε can be additively decomposed into an elastic term, ε_e, and a plastic one, ε_p. The plasticity condition is determined through a scalar yield function f in the stress space, where the elastic domain is defined by stress states with $f < 0$ and the plastic flow or elastic unloading occurs when $f = 0$, based on the total strain rate $\dot{\varepsilon}$ parameter. This methodology solves for stress component in a two-step procedure, the first phase assumes an elastic trial step and second one, a plastic corrector. The procedure is summarized in Fig. 5.

1. Compute ε.
2. Set:
   $\Delta\lambda = 0$
   $\varepsilon_p = \varepsilon_{p,old}$
   $\bar{\varepsilon}_p = \bar{\varepsilon}_{p,old}$
   $\alpha = \alpha_{old}$
   $\sigma_y = \sigma_{y,old}$
3. Compute $\sigma = E(\varepsilon - \varepsilon_p)$
4. Compute $f = |\sigma - \alpha| - \sigma_y$
5. If ($f < 0$)
   Assign all values as the new state.
   Else
   While ($f \neq 0$)
   $\Delta\lambda = f/(E + H_{iso} + H_{kin})$
   $\varepsilon_p = \varepsilon_p + \Delta\lambda \cdot \text{sign}(\sigma - \alpha)$
   $\alpha = \alpha + H_{kin} \cdot \Delta\lambda \cdot \text{sign}(\sigma - \alpha)$
   $\bar{\varepsilon_p} = \bar{\varepsilon_p} + \Delta\lambda$
   $\sigma_y = \sigma_y + H_{iso} \cdot \Delta\lambda$
   $\sigma = \sigma - E \cdot \Delta\lambda \cdot \text{sign}(\sigma - \alpha)$
   $f = |\sigma - \alpha| - \sigma_y$
   End
   End

Figure 5. Returning map algorithm.

3. RESULTS

As previous explained, we seek to study the dynamic behavior of the von Mises truss under a set of distinct load time histories, and its pseudo-static response using different cross-sections, material and load conditions. For this we use the proposed procedures presented in section 2 and the non-dimensional set of equations obtained in section 1, Eq. (6) and Eq. (7).

For all simulations, we have used the following constant parameters: initial length $l_0 = 1.0$, height $a = 0.2$, cross-section area $A_0 = 0.0125$, elastic modulus $E = 1e4$, isotropic hardening moduli $H_{iso} = 1e3$, kinematic hardening moduli $H_{kin} = 1e3$, initial yield stress $\sigma_y, 0 = 1e2$ and mass $m = 1$. Based on those, we define the following non-dimensional variables: static load $\eta = [-1, 0]$, frequency $\Omega = [0.02, 0.2, 2]$, dynamic non-dimensional load $\gamma = [-0.01, 0]$ and damping ratio $\xi = [0.05, 0.15]$. Finally, we study three possible sets of initial conditions, $\dot{x}$ and x non-null; $\dot{x}$ null and x no-null; and $\dot{x}$ non-null and x null.

In the first simulation, we perform a comparative analysis of the two most generally known incremental iterative procedures, the Newton-Raphson and the Arc-length method, see Fig. 6.

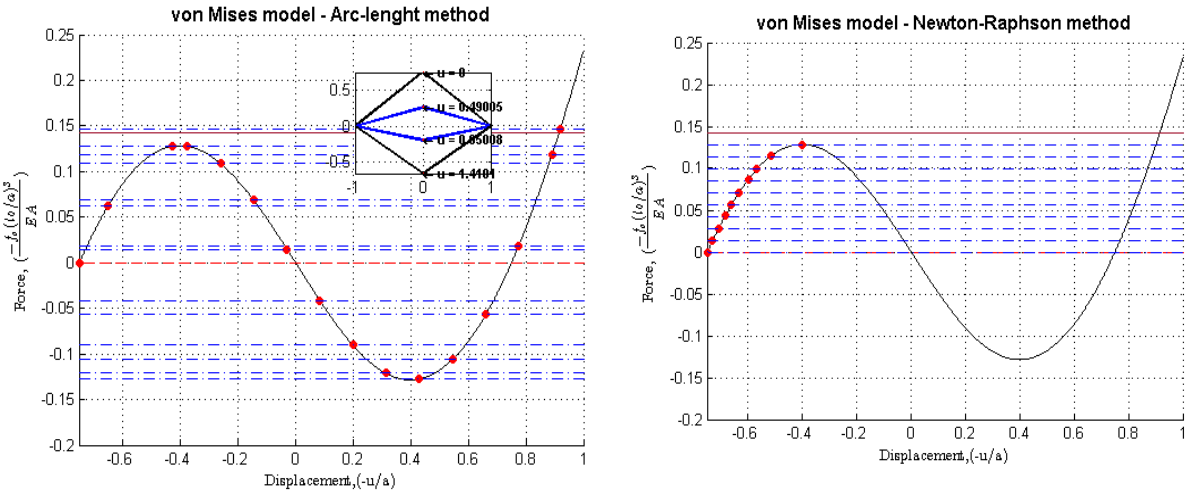

Figure 6. Static response of the von Mises structure for different incremental iterative procedures, the left curve being the Arc-length method and the right one the full Newton-Raphson.

From Figure 6, it is possible to notice that near limit points, where the tangent stiffness matrix becomes singular, the Newton-Raphson procedure fails in finding a new equilibrium point. A possible solution for this problem is the adoption of smaller increments near the limit point or adopt the modified Newton-Raphson method – where the tangent stiffness matrix is updated in specific conditions, seeking to avoid the singularity. On the other hand, path-following methodologies, such as the arc-length method does not find any difficulties in trace the nonlinear load displacement curve of the model, as shown in the left graph. Thus, justifying its use in the current version of our code.

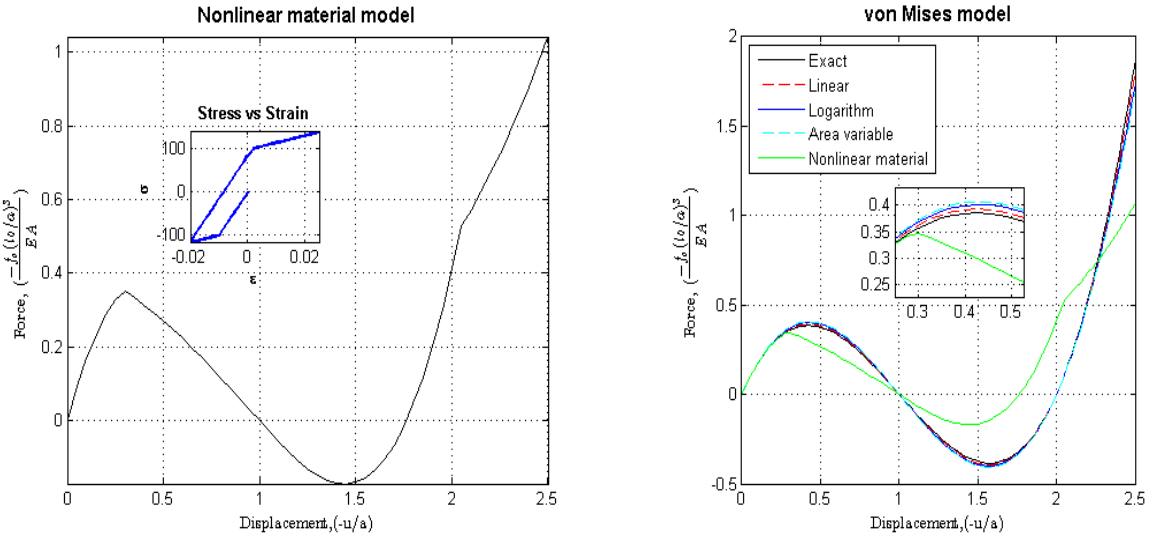

Figure 7. Static nonlinear force x displacement curves of the von Mises structure, the left curve being a nonlinear material analysis and the right one the comparison between some typical stress strain relations.

The impact of nonlinearities in the final response of the von Mises truss can be easily identified in the curves of Fig. 7, where the adoption of an One-Dimensional J2 (von Mises) Plasticity model can anticipate the unstable response of the structure, as show in the left curve of Fig.7. Furthermore, the adoption of different kinds of stress strain relation can have considerable impact in the static response of models undergoing large displacements, as shown in the early detachment of the linear and logarithm curve from the exact solution.

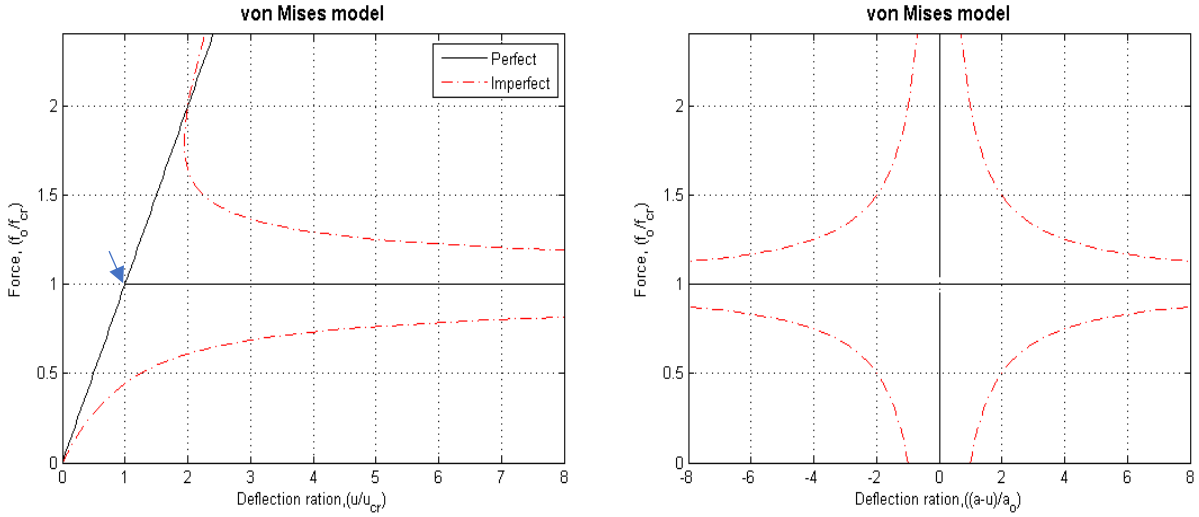

Figure 8. Load/deflection relationships for the two-dimensional von Mises structure, where the left curve is the transverse deflection and the right one the shortening deflection.

Figure 8 presents the static solution for the two variables model of the von Mises structure. In this simulation, the perfect system solution is achieved when the vertical variable is set to zero. In this case, the system remains stable until the point A (represented as an arrow in the left curve), from which the horizontal path is the post-buckling condition. If the offset,u, is non-zero, the imperfect curve will be followed (red curve). In addition, the right curve of Fig. 8 presents the shortening deflection of the model, with the black curve representing the response for the perfect system and the red one for a non-zero offset.

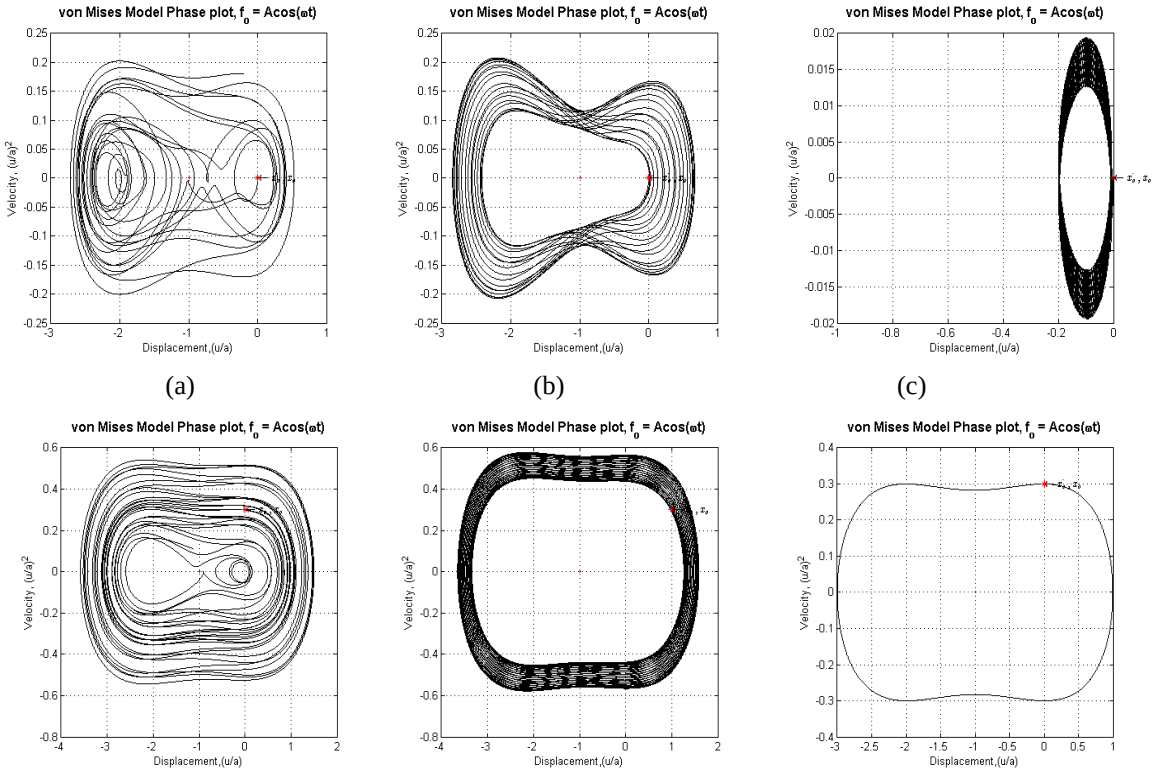

Figure 9. Phase plots of the von Mises structure for different parameters and initial conditions, where (a),(b),(c) are the phase plot of the undamped system with null initial conditions and different set of frequencies and (d),(e) and (f) the undamped system with non-null initial conditions and fixed frequency.

In the dynamic context, we can notice the similarity between the non-dimensional form of Eq. (7) and the motion equation of the duffing oscillator and hence understanding the rich dynamic behaviors of this model. For a periodic load given by $\gamma\cos(\Omega\tau)$ and undamped conditions, we have the three phase plot curves presented in upper part of Fig. 9 (a-c). The first plot represents the dynamic response for forcing frequency $\Omega = 0.2$, with complex motions concentrated near the second equilibrium position ($u = 2a$). Phase plot (b) represents a dynamic response for a lower forcing frequency value ($\Omega = 0.02$), showing that for this condition the motion is more well-behaved but still oscillating between the two equilibrium points. Finally, for a higher frequency, $\Omega = 2$, the dynamic response oscillates around the first equilibrium node.

For a free vibration and undamped condition – the curves presented in Fig. 9 (d-f) – we notice that the different sets of initial conditions ($\dot{x}$ non-null and x null; $\dot{x}$ and x non-null; and $\dot{x}$ null and x no-null, respectively) do not alter the final shape of the phase plot. The main difference between these three sets of conditions is that the additional energy, originated from the non-null velocity, leads to a better described curve, as shown in Fig.9 (e) and (f).

Figure 10 takes into account the damping effects, leading to phase plots typical of damped systems. The upper set of curves (Fig. 10 (a)-(c)) represents the periodic load simulation showing the impact of different frequencies in the final response. As we can see, for a frequency equals $\Omega = 0.2$, the system circles around the first equilibrium position ($u = a$), while a lower frequency changes the equilibrium point to the second equilibrium position. For a higher frequency the response is similar to the undamped one, oscillating around the first configuration.

The last four curves, Fig. 10 (d)-(f), exemplify the impact of different initial conditions and two values of ξ, showing that for a free vibration damped system the response always converge to an equilibrium configuration. Finally, it should be noted that for initial conditions with more energy, the system can oscillate through the unstable region before converging to a equilibrium condition.

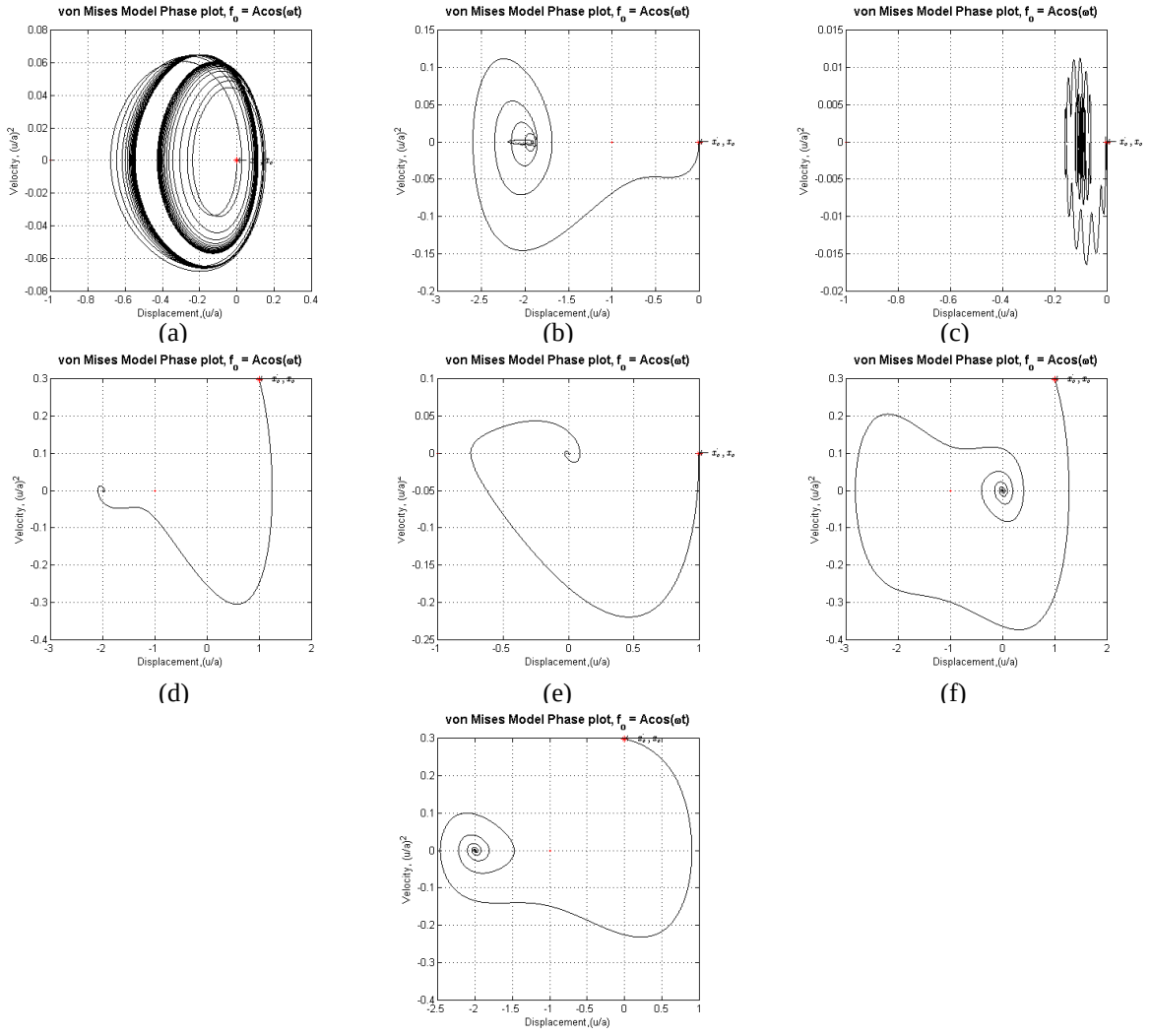

Figure 10. Phase plots of the von Mises structure for different parameters and initial conditions, where (a),(b),(c) are the phase plot of the damped system with null initial conditions and fixed frequency; (d),(e) are the free vibration system with $\xi = 0.05$ and (f), (g) the free vibration system with $\xi = 0.15$.

4. CONCLUSIONS

A nonlinear numerical study of the von Mises structure was carried out to describe its dynamic behavior under a set of distinct load time histories, since it is well known that this problem may lead, for certain parameters and initial conditions, to chaotic solutions, among other rich dynamic behaviors, thus justifying this nonlinear analysis in the dynamic context. As presented in Fig. 7, 8 and 9; the nonlinear static analysis shows some limitations of the displacement-control, or load-control methodologies, as well as, the impact of some nonlinear considerations in the static response. Moreover, those curves are the same found in the literature (see Crisfield (1991), Krenk (2009) and Reddy (2004)), confirming our algorithm precision and performance in some simple nonlinear examples. In the dynamic nonlinear context, we notice the similarity between the von Mises motion equation and the Duffing oscillator, such similarity confirmed by the rich dynamic behavior. The variation of frequency, magnitude, initial conditions and damping can lead to different equilibrium states based on the amount of energy applied and absorbed by the system, the main example being the curves from Fig. 10, where the initial conditions applied led to different equilibrium configurations.

5. ACKNOWLEDGEMENTS

This research was supported by CAPES (Coordenação de Aperfeiçoamento de Pessoal de Nível Superior). The second author also acknowledges support by CNPq.

6. REFERENCES

Bathe, Klaus-Jürgen; M. Irfan Baig, Mirza. “Conserving energy and momentum in nonlinear dynamics:A simple implicit time integration scheme”. *Computers & Structures*, 85, 437-445, 2007.

Brasil, R.M.L.R.F. *Não-Linearidade Geométrica na Dinâmica de Estruturas Aporticadas Planas: Um Tratamento Pelo Método dos Elementos Finitos*. Thesis (Doutorado em Engenharia Civil) - Universidade de São Paulo (USP), 1990.

Carrera, E. “A Study on Arc-length-type Methods and their Operation Failures Illustrated by a Simple Model”. *Computers and Structures*, Vol. 50 (2), p. 217-229, 1994.

Crisfield, M. A. *Non-linear Finite Element Analysis of Solids and Structures, Volume 1: Essentials*. John Wiley & Sons, England, 1991.

Crisfield, M. A. *Non-linear Finite Element Analysis of Solids and Structures, Volume 2: Advanced Topics*. John Wiley & Sons, England, 1997.

Conte, J. P. et.al. “Consistent Finite-Element Response Sensitivity Analysis”. *Journal of Engineering Mechanics*, Vol. 129, Issue 12, 1380-1393, 2003.

Driemeier, L. et.al. “A contribution to the numerical nonlinear analysis of three-dimensional truss systems considering large strains, damage and plasticity”. *Communications in Nonlinear Science and Numerical Simulation*, 10, 515:535, 2005.

Krenk, S. *Non-linear Modeling and Analysis of Solids and Structures*. Cambridge: Cambridge University Press, 2009.

Ligarò, S.S. & Valvo, P.S. “Large displacement analysis of elastic pyramidal trusses”. *International Journal of Solids and Structures*, Vol.43, Issue 16, Pgs. 4867-4887, 2006.

Memon, BA. & Su, X. J. “Arc-length technique for nonlinear finite element analysis”. *Journal of Zhejiang University SCIENCE*, 5: 618, 2004. https://doi.org/10.1631/jzus.2004.0618

Neto, E. A. de Souza. *Computational methods for plasticity: theory and applications*. Chichester, West Sussex, United Kingdom, Wiley, 2008.

Pimenta, P. M. “Análise Não Linear de Treliças Espaciais”, Escola Politécnica da Universidade de São Paulo, Universidade de São Paulo, *Boletim Técnico BT/PEF-8604*, 1983.

Reddy, J. N. *An Introduction to Nonlinear Finite Element Analysis*, Oxford University Press, Oxford, UK, 2004.

Savi, M.A. et.al. “Chaos in a shape memory two-bar truss”.*International Journal of Non-Linear Mechanics*, 37, 1387–1395, 2002.

Souza, L.A.F. et al. “Trusses Nonlinear Problems Solutions with Numerical Methods of Cubic Convergence Order”. *Tendências em Matemática Aplicada e Computacional*, 19, N.1 (2018), 161-179.

Souza Lima, V.; Brasil, R. M. L. R. F. “On the Geometrically Nonlinear Analysis of Trusses”. *In: Thematic Conference On Computational Methods,* 1998, Barcelona. Proceedings. Barcelona: CIMNE, 1998.

7. RESPONSIBILITY NOTICE

The authors are the only responsible for the printed material included in this paper.